# Dalton Transactions

Accepted Manuscript






ROYAL SOCIETY OF CHEMISTRY

www.rsc.org/dalton

## Graphical Abstract

**Halogen substituent effects on the spin crossover behaviour of Fe(III) quinolylsalicylaldimine complexes**

Wasinee Phonsri, David J. Harding,* Phimphaka Harding, Keith S. Murray, Boujemaa Mourabaki, Ian A. Gass, John D. Cashion and Harry Adams

Four iron(III) spin crossover complexes with halogen substituted ligands are reported. The halogen is correlated with $T_{½}$ and controls the degree of spin crossover while extensive C-H···X and X···π interactions increase cooperativity.

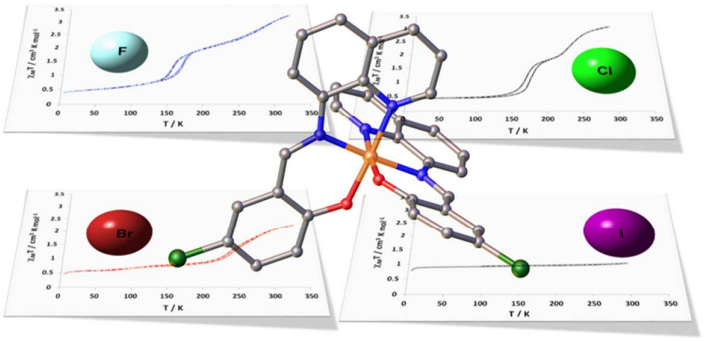

Dalton Transactions RSCPublishing

# Stepped spin crossover in Fe(III) halogen substituted quinolylsalicylaldimine complexes

Cite this: DOI: 10.1039/x0xx00000x

Wasinee Phonsri,[a,b] David J. Harding,*[a] Phimphaka Harding,[a] Keith S. Murray,[b] Boujemaa Mourabaki,[b] Ian A. Gass,[b,c] John D. Cashion,[d] Guy N. L. Jameson[e] and Harry Adams[f]

Received ooth January 2012,
Accepted ooth January 2012

DOI: 10.1039/x0xx00000x

www.rsc.org/

The reaction of $Fe(NCS)_3$ prepared *in situ* in MeOH with Hqsal-X (Hqsal-X = 5-X-*N*-quinolylsalicylaldimine) in $CH_2Cl_2$ yields the $Fe^{III}$ complexes, $[Fe(qsal\text{-}X)_2]NCS{\cdot}solvent$ (X = F **1**; X = Cl, **2**, Br, **3** solvent = MeOH; X = I, solvent = $0.25CH_2Cl_2{\cdot}0.5MeOH$ **4**) in moderate to good yields. IR spectroscopy confirms that $NCS^-$ acts as a counteranion only and that the qsal-X ligand is bound to the $Fe^{III}$ centre. SQUID magnetometric studies reveal stepped hysteretic spin crossover in **1** and **2**, which is abrupt in both steps in latter compound. Mössbauer spectroscopic studies of **1** and **2** support these conclusions. The bromo derivative, **3**, undergoes half spin crossover up to 340 K while **4** is low spin at all temperatures measured. The spin transition temperature, $T_{½}$ is found to increase on moving from F to Br. UV-Vis and NMR spectroscopic studies indicate that **1**-**4** have spin states intermediate between HS and LS in solution. Structural studies show that **1**, **2** and **3** crystallize in triclinic $P\bar{1}$ while **4** is in monoclinic $P2_1/c$. Crystallographic studies of **1** at 100, 200 and 270 K show that spin crossover proceeds from a [LS-LS] state through a [LS-HS] intermediate to a [HS-HS] state (LS = low spin, S= 1/2, HS = high spin, S = 5/2) . Similar results are found for **3** although this time a [LS-IS] state exists at 123 K while a [LS-HS] state is found at 295 K (IS = intermediate spin state where partial spin has occurred). Both **2** and **4** are found to have LS $Fe^{III}$ centres although the latter contains two crystallographically independent $Fe^{III}$ centres in the asymmetric unit. The crystal packing in **1**-**4** consists of extensive π-π interactions through the planar qsal-X ligands and CH···X (X = O, halogen) and/or X···π (X = halogen) interactions which result in *pseudo* 3D supramolecular networks. This results in high cooperativity in **1** and **2** and is probably responsible for the hysteretic stepped spin crossover in these compounds.

## Introduction

Molecular bistability is a much sought after property in transition metal based materials as a result of the many potential applications these materials may have including molecular switches, sensors and data storage devices.[1–4] One of the most elegant examples of bistability is spin crossover (SCO) in which the bistability relies on switching from a high spin (HS) to a low spin (LS) state.[1] A particular advantage of spin crossover materials is that the switching may be achieved by changes in temperature,[1,2] pressure[5] or, more rarely, light.[6,7] However, while spin crossover is theoretically possible for any complex with a suitable ligand field possessing a $d^4$-$d^7$ electron configuration, it is most widely studied in $d^5$ and $d^6$ systems as these exhibit the largest structural and magnetic changes.[1,2] In this regard $Fe^{III}$ ($d^5$) undergoes spin crossover from a HS state (S = 5/2) to a LS state (S = 1/2) typically utilizing an $N_4O_2$ donor set.[8,9] Several ligand types are known but the two most common are hexadentate ligands such as $H_2sal_2trien$ ($H_2sal_2trien$ = N,N′′′-bis(salicylidene)-1,4,7,10-tetraazadecane) and tridentate ligands in which two ligands are needed to achieve the required octahedral geometry.[8,9] Although a wide variety of tridentate ligands have been used, many are Schiff bases such as *N*-quinolylsalicylaldimine (Hqsal) which has been used to prepare $[Fe(qsal)_2]NCSe{\cdot}solvent$ (solvent = DMSO, $CH_2Cl_2$, MeOH), spin crossover complexes exhibiting abrupt spin crossover with hysteresis varying from 70-76 K.[10,11] This discovery led to an explosion in research concerning $Fe^{III}$ spin crossover complexes but has focused almost exclusively on changing the anion.[12–15] More recently, we have been exploring substituted qsal ligands and have found that abrupt and stepped spin crossover with hysteresis can be achieved.[16–18] Despite the above successes, studies of the effect that substituent groups have on spin crossover are still poorly developed. One of the few systems to be studied in $Fe^{III}$ chemistry is [(TpyA)Fe(cat-R)]Y (TpyA = tris(2-pyridylmethyl)amine, cat-R = substituted catecholate: R = 4-methyl, 3-methoxy, 3,4,5,6-tetrachloro, 4,5-dinitro; Y =

anion).[19] However, within this series only one SCO active pair was structurally characterized severely restricting any conclusions that might be drawn regarding the structure:function relationship[20] of these compounds. Moreover, the different positions of the substituent groups, their very different electronic properties and shapes, perhaps explain the lack of any clearly defined pattern in the SCO behaviour. In seeking to address this issue we have prepared a series of halogen substituted spin crossover complexes [Fe(qsal-X)$_2$]NCS·solvent (X = F; X = Cl, Br, solvent = MeOH; X = I, solvent = 0.25$CH_2Cl_2$·0.5MeOH) where the halogen group remains in the same position and the anion is kept constant. Halogen substituents were chosen with the aim of introducing halogen···π and halogen bonding interactions in the hope of increasing the cooperativity.[21] In this report we structurally characterize all the compounds, in some cases at multiple temperatures, allowing us to directly link how subtle changes in this single substituent group in combination with solvent effects impact the structure and thus the magnetic performance of the compounds.

## Results and discussion

### Synthesis of [Fe(qsal-X)$_2$]NCS

The complexes [Fe(qsal-X)$_2$]NCS·solvent (X = F **1**; X = Cl, **2** Br, **3** solvent = MeOH; X = I, solvent = 0.25$CH_2Cl_2$·0.5MeOH **4**) were prepared by carefully layering a solution of $Fe(NCS)_3$ in MeOH over a solution of the ligand, Hqsal-X in $CH_2Cl_2$ in which $NEt_3$ had been added. The compounds are black and slightly soluble in polar solvents (Scheme1).

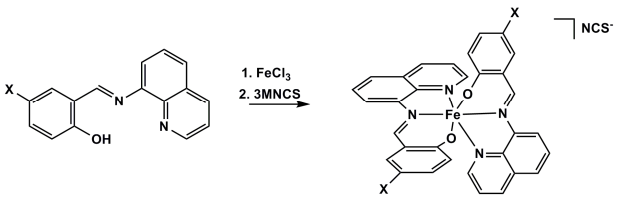


**Scheme 1** Synthesis of [Fe(qsal-X)$_2$]NCS·solvent.

IR spectroscopy shows strong $\nu_{C\equiv N}$ stretches for the $NCS^-$ anion between 2057-2055 $cm^{-1}$ and consistent with an unbound NCS counteranion.[18,22]

**Table 1** Physical and IR spectroscopic data for [Fe(qsal-X)$_2$]NCS·solvent.

| Compound | Colour | Yield (%) | IR ($cm^{-1}$)[a] | |
|---|---|---|---|---|
| | | | $\nu_{C\equiv N}$ | $\nu_{C=N}$ |
| **1** | Black | 79 | 2057 | 1600 |
| **2** | Black | 33 | 2056 | 1601 |
| **3** | Black | 34 | 2055 | 1600 |
| **4** | Black | 49 | 2056 | 1599 |

[a]As KBr discs.

There are also clear stretches assignable to the imine C=N bond of the qsal-X ligand being *ca.* 15 $cm^{-1}$ lower than the free ligand[23] and consistent with coordination to the $Fe^{III}$ centre (Table 1).

### Magnetic studies of [Fe(qsal-X)$_2$]NCS·solvent

To explore the magnetic properties of the different complexes we undertook magnetic susceptibility studies using SQUID magnetometry between 4-340 K. The results are shown in Figure 1. The $\chi_M T$ value for **1**, **2** and **3** is *ca.* 0.45 $cm^3$ K $mol^{-1}$ at 5 K and consistent in all cases with a LS $Fe^{III}$ centre as reported in related $[Fe(qsal\text{-}X)_2]^+$ compounds ($\chi_M T$ = 0.375 $cm^3$ K $mol^{-1}$ for LS $Fe^{III}$).[16–18] For **1**, upon heating, the $\chi_M T$ value gradually increases to *ca.* 0.80 $cm^3$ K $mol^{-1}$ at 140 K before increasing moderately abruptly, reaching *ca.* 1.90 $cm^3$ K $mol^{-1}$ at 200 K, before becoming more gradual again to reach a final value of 3.26 $cm^3$ K $mol^{-1}$ at 340 K and consistent with 72% of the Fe centres being HS (assuming $\chi_M T$ = 4.375 $cm^3$ K $mol^{-1}$ for HS $Fe^{III}$; $\chi_M T = \gamma(4.375) + 1\text{-}\gamma(0.375)$, γ = %HS; see Table 2). However, it should be noted that both [Fe(qsal)$_2$]NCY (Y = S, Se) are fully HS at *ca.* 4.0 $cm^3$ K $mol^{-1}$, a little lower than the expected value of 4.375 $cm^3$ K $mol^{-1}$ and may suggest that the HS fraction is underestimated, something Mössbauer spectroscopic data confirms (*vide infra*).

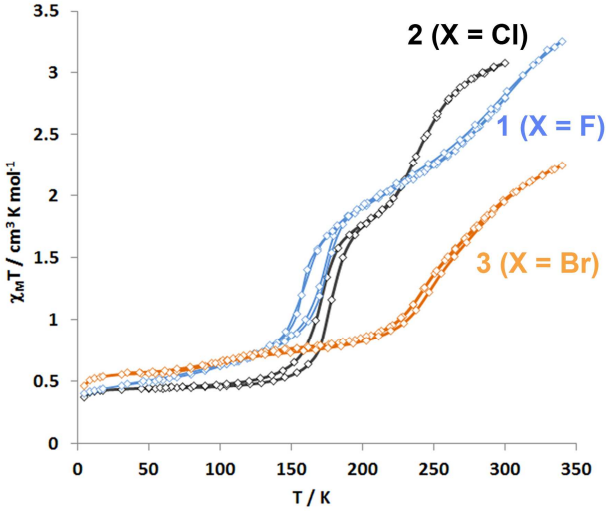


**Figure 1** Thermal variation of $\chi_M T$ versus T plot for **1**, **2** and **3**.

Cooling the sample results in the $\chi_M T$ value decreasing following the heating curve until at *ca.* 180 K the two curves diverge before re-joining the heating curve at 140 K. The above results are indicative of spin crossover in two steps with hysteresis in the 1st step of *ca.* 13 K. The chloro derivative, **2** shows a very similar magnetic profile to **1**, although in this case the spin crossover is more abrupt meaning that the plateau region around 210 K is more clearly defined. Once again there is hysteresis in the 1st step, this time of 10 K, and the final $\chi_M T$ value of 3.10 $cm^3$ K $mol^{-1}$ indicates that the compound is *ca.* 68% HS. Although a number of other $[Fe(qsal\text{-}X)_2]^+$ complexes are known to undergo stepped SCO,[10,11,17] this is the first time that stepped SCO through a 50% HS-LS intermediate has been observed. Interestingly, [Fe(qsal)$_2$]NCS also exhibits stepped SCO, in this case via a 33% HS intermediate and only in the warming mode with a hysteresis ranging from 87 to 7 K.[22,24]

In contrast to the stepped hysteretic spin crossover observed in **1** and **2**, the spin crossover in **3** is much more gradual reaching *ca*. 0.90 $cm^3$ K $mol^{-1}$ at 210 K before increasing more rapidly, finally reaching 2.25 $cm^3$ K $mol^{-1}$ at 340 K and indicative of 47% of the $Fe^{III}$ centres being HS. While **1**, **2** and **3** all show spin crossover, the magnetic response of **4** is invariant at all temperatures studied with a $\chi_M T$ value of 0.90 $cm^3$ K $mol^{-1}$ and slightly higher than would be expected for a pure LS system (see Figure S1).

Looking at the $T_{½}$ values for the F and Cl derivatives and the clear 50% SCO in **3**, we find that the transition temperature increases as we descend the group. It would appear from solution experiments (*vide infra*) that the size of the halogen and the different solvent molecules and their effect on the lattice are responsible for this trend. Comparing **1**-**3** with $[Fe(qsal)_2]NCS$ the latter compound has a wider hysteresis suggesting that introduction of the halogen decreases the overall cooperativity in the structure.[22,24]

**Table 2** Experimental transition temperatures for **1**-**3** in K.

| Compound | $T_{½}\uparrow$ | $T_{½}\downarrow$ | $\Delta T$ |
|---|---|---|---|
| **1** | 170 | 157 | 13 |
| **2** | 177 | 167 | 10 |
| **3** | - | - | - |
| **$[Fe(qsal)_2]NCS$**[a] | 290 | 203 | 87[b] |
| | 210 | 203 | 7[b] |

[a] Data from ref. 22. [b]At the widest point.

It is well known that the magnetic state of spin crossover complexes in solution is often very different to that in the solid state.[25] Thus, the spin state was determined in DMSO using the Evans' method.[26–28] The spin state is found to be intermediate between HS and LS in all cases varying from 22-49% HS (see Figure S2, Table S1). Although, there is no correlation between the electro-negativity or size of the halogens it is clear that the halogen *does* impact the ligand field and consequently the spin state of the complex. However, these relatively minor changes in spin state indicate that the different solid state SCO characteristics result principally from changes in the crystal lattices which are influenced by both the halogen and solvent molecules. UV-Vis spectra of **1**-**4** also recorded in DMSO reveal two peaks at *ca*. 330 and 420 nm and are assigned to π-π* and LMCT transitions, respectively (Figure S3).[16,17,29] In the spectra there is also a shoulder at *ca*. 800 nm which by comparison with $[Fe(qsal\text{-}C{\equiv}C\text{-}3\text{-}th)_2]^+$ (3-th = 3-thienyl) is attributed to the LS species (Figure S4).[29]

### Structural studies of $[Fe(qsal\text{-}X)_2]NCS{\cdot}solvent$

Crystals of all complexes were grown by slow diffusion of the ligand in $CH_2Cl_2$ into a solution of $Fe(NCS)_3$ in MeOH over 3-5 days. The crystals of **1** diffracted very weakly and synchrotron radiation was required to get suitable data. The structure of **1** was collected at 100, 200 and 270 K while **2** was collected at 100 K, and **3** was determined at 123 and 295 K with **4** collected at 123 K. Sadly, we've been unable to explore **2** at higher temperatures due to loss of crystallinity (not due to solvent loss as shown by TGA, Figure S5). The compounds all crystallize in the triclinic space group P$\bar{1}$ with the exception of **4** which crystallizes in monoclinic $P2_1/c$. By comparison, $[Fe(qsal)_2]NCS{\cdot}CH_2Cl_2$ crystallizes in triclinic P$\bar{1}$ while $[Fe(qsal)_2]NCS$ is in monoclinic $P2/n$.[22] The structures of **1**, **3** and **4** reveal two crystallographically independent $Fe^{III}$ centres in the asymmetric unit along with MeOH and/or $CH_2Cl_2$ solvent molecules for **3** and **4** (Figure 2).

**Table 3** Selected Fe-N/O bond lengths (Å) and octahedral distortion parameters (°).

| | **1** | | | **2** | **3** | | **4** |
|---|---|---|---|---|---|---|---|
| | **100 K** | **200 K** | **270K** | **100 K** | **123 K** | **295 K** | **123 K** |
| Fe1-O1 | 1.876(2) | 1.873(1) | 1.870(2) | 1.876(4) | 1.866(4) | 1.873(4) | 1.870(4) |
| Fe1-O2 | 1.864(2) | 1.863(1) | 1.861(2) | 1.872(4) | 1.882(4) | 1.872(4) | 1.877(4) |
| Fe1-$O_{av}$ | 1.870(2) | 1.868(1) | 1.866(2) | 1.874(4) | 1.874(4) | 1.873(4) | 1.874(4) |
| Fe1-N1 | 1.947(2) | 1.946(1) | 1.969(2) | 1.982(5) | 1.944(5) | 1.942(4) | 1.953(5) |
| Fe1-N2 | 1.978(2) | 1.979(2) | 2.000(2) | 1.962(5) | 1.970(5) | 1.969(5) | 1.944(4) |
| Fe1-N3 | 1.942(2) | 1.941(2) | 1.964(2) | 1.970(5) | 1.939(4) | 1.938(4) | 1.944(4) |
| Fe1-N4 | 1.972(2) | 1.977(2) | 1.999(2) | 1.941(5) | 1.973(5) | 1.974(5) | 1.963(5) |
| Fe1-$N_{av}$ | 1.960(2) | 1.961(2) | 1.983(2) | 1.964(5) | 1.956(5) | 1.956(5) | 1.951(5) |
| Fe2-O3 | 1.871(2) | 1.896(2) | 1.895(2) | | 1.902(4) | 1.907(4) | 1.875(4) |
| Fe2-O4 | 1.879(2) | 1.900(2) | 1.900(2) | | 1.912(4) | 1.917(4) | 1.877(4) |
| Fe2-$O_{av}$ | 1.875(2) | 1.898(2) | 1.899(2) | | 1.907(5) | 1.912(4) | 1.876(4) |
| Fe2-N5 | 1.952(2) | 2.113(2) | 2.113(2) | | 2.072(6) | 2.118(5) | 1.948(5) |
| Fe2-N6 | 1.978(2) | 2.139(2) | 2.141(2) | | 2.102(6) | 2.162(5) | 1.959(5) |
| Fe2-N7 | 1.953(2) | 2.112(2) | 2.115(2) | | 2.065(5) | 2.124(5) | 1.948(4) |
| Fe2-N8 | 1.978(2) | 2.134(2) | 2.135(2) | | 2.112(5) | 2.153(5) | 1.967(5) |
| Fe2-$N_{av}$ | 1.965(2) | 2.125(2) | 2.126(2) | | 2.088(6) | 2.139(5) | 1.956(6) |
| $\Sigma^a$-Fe1, Fe2 | 43, 51 | 40, 73 | 40, 73 | 48 | 47, 61 | 47, 77 | 54, 53 |
| $\Theta^b$-Fe1, Fe2 | 62, 81 | 59, 198 | 71, 198 | 67 | 62, 165 | 65, 213 | 81, 80 |

[a] See ref. 24 for a definition. [b] See ref. 25 for a definition.

The presence of two independent $Fe^{III}$ centres, while unusual, is also found in $[Fe(qsal)_2]NCSe$.[10] Interestingly, **2** is found to have only one $Fe^{III}$ centre in the asymmetric unit at 100 K and, while apparently inconsistent with the stepped SCO observed in the magnetic studies, is not unprecedented with $[Fe(qsal)_2]NCS$ also showing similar behaviour, albeit via a 33% HS

intermediate.[22] The reason for the stepped SCO is explained in more detail below.

At 100 K the Fe-N/O bond lengths in $[Fe(qsal\text{-}F)_2]NCS$ are on average 1.963 Å and 1.873 Å, respectively and consistent with LS $Fe^{III}$ centres in both cases.[16,17,30]

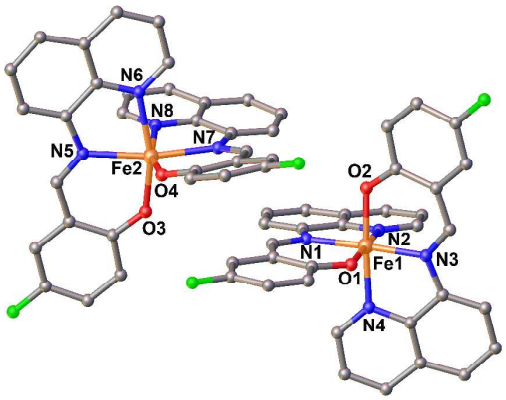


**Figure 2** View of the asymmetric unit in $[Fe(qsal\text{-}F)_2]NCS$ **1** showing the HS (Fe2) and LS (Fe1) $Fe^{III}$ centres and partial atomic numbering at 200 K. Hydrogen atoms and the two NCS anions are omitted.

Heating to 200 K results in little change in the Fe1-N/O bond lengths (see Table 3). However, the Fe2-N/O bond lengths increase by 0.02 and 0.16 Å, respectively and are indicative of spin crossover at the Fe2 centre.[16,17] At 270 K the coordination sphere of Fe2 remains unchanged but there is now a slight change in the Fe1-N/O bond distances and, more tellingly, a subtle difference in the octahedral distortion parameter, Θ suggesting the onset of spin crossover in Fe1.[31,32] This directly parallels the magnetic susceptibility studies and indicates that the stepped SCO in **1** results from the presence of crystallographically independent Fe centres and thus proceeds from a [LS-LS] state through a [LS-HS] intermediate to a [HS-HS] state at high temperatures. This is the first *structural* proof of stepwise spin crossover in $[Fe(qsal\text{-}X)_2]^+$ chemistry.

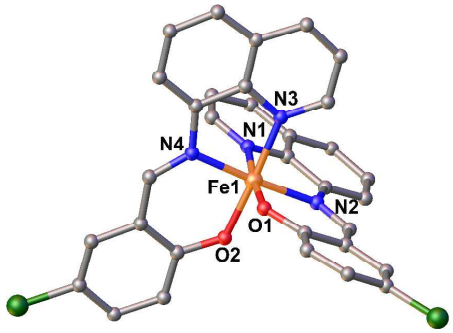


**Figure 3** View of the asymmetric unit in $[Fe(qsal\text{-}Cl)_2]NCS{\cdot}MeOH$ **2** showing partial atomic numbering.

**Table 4** Crystallographic data and structure refinement for **1**-**4**.

| | **1** | | | **2** | **3** | | **4** |
|---|---|---|---|---|---|---|---|
| | **100 K** | **200 K** | **270 K** | **100 K** | **123 K** | **295 K** | **123 K** |
| Formula | $C_{33}H_{20}F_2FeN_5O_2S$ | | | $C_{34}H_{24}Cl_2FeN_5O_3S$ | $C_{34}H_{24}Br_2FeN_5O_3S$ | | $C_{67.5}H_{45}ClFe_2I_4N_{10}O_5S_2$ |
| Molecular weight / $gmol^{-1}$ | 644.45 | | | 709.39 | 798.31 | | 1792.38 |
| Crystal system | Triclinic | Triclinic | Triclinic | Triclinic | Triclinic | Triclinic | Monoclinic |
| Space group | P1 | P1 | P1 | P1 | P1 | P1 | $P2_1/c$ |
| *a* / Å | 9.870(2) | 9.849(2) | 9.919(2) | 10.0244(12) | 10.1777(6) | 10.3118(6) | 20.8247(10) |
| *b* / Å | 11.998(2) | 12.100(2) | 12.084(2) | 12.1032(14) | 12.7832(8) | 12.8729(8) | 23.9937(11) |
| *c* / Å | 23.533(5) | 23.856(5) | 23.951(5) | 13.0961(16) | 25.5491(18) | 25.6592(16) | 12.6558(5) |
| α / ° | 98.97(3) | 99.39(3) | 99.55(3) | 105.652(7) | 76.095(2) | 76.441(2) | 90.00 |
| β / ° | 99.89(3) | 99.45(3) | 99.39(3) | 97.910(8) | 79.175(3) | 79.516(2) | 91.1070(10) |
| γ / ° | 90.65(3) | 90.81(3) | 90.62(3) | 98.813(7) | 77.517(2) | 77.756(2) | 90.00 |
| T / K | 100(2) | 200(2) | 270(2) | 100(2) | 123(2) | 295(2) | 123(2) |
| Cell volume / $Å^3$ | 2709.7 (9) | 2764.4(10) | 2791.0(10) | 1485.0(3) | 3117.8(3) | 3204.3(3) | 6322.4(5) |
| *Z* | 4 | 4 | 4 | 2 | 4 | 4 | 4 |
| Absorption coefficient / $mm^{-1}$ | 0.691 | 0.677 | 0.671 | 0.805 | 3.159 | 3.074 | 2.581 |
| Reflections collected | 87868 | 100614 | 102859 | 23398 | 20532 | 21439 | 43766 |
| Independent reflections, $R_{int}$ | 11823, 0.0588 | 15562, 0.0318 | 15635, 0.0312 | 6678, 0.0993 | 13875, 0.0350 | 14503, 0.0356 | 14538, 0.0524 |
| Max. and min. transmission | - | - | - | 0.9762 and 0.8427 | 0.623 and 0.403 | 0.631 and 0.414 | 0.3896 and 0.6981 |
| Restraints /parameters | 30/821 | 6/816 | 42/812 | 0/417 | 0/833 | 0/826 | 76/905 |
| Final R indices [$I>2\sigma(I)$]: $R_1$, $wR_2$ | 0.0496, 0.1285 | 00463, 0.1294 | 0.0540, 0.1589 | 0.0818, 0.2156 | 0.0684, 0.1639 | 0.0631, 0.1907 | 0.0461, 0.1167 |

The structure of **2** reveals short Fe-N/O bond lengths characteristic of LS $Fe^{III}$ and consistent with the SQUID magnetometric studies above (Figure 3).[33] The Fe centre is also very regular and resembles that of the Fe1 centre in **1** (Table 3). In contrast to **2**, $[Fe(qsal\text{-}Br)_2]NCS{\cdot}MeOH$ is characterized by two crystallographically distinct Fe centres. At 123 K the Fe1-

N/O bond lengths vary between 1.938-1.972 Å and 1.872-1.876 Å, respectively and are in the range reported for other $Fe^{III}$ LS centres. The Fe2 centre has Fe-N/O bond lengths that average 2.088 and 1.908 Å, respectively. These are intermediate between the values expected for a HS and LS $Fe^{III}$ centre and suggest that at this temperature we have an intermediate spin state denoted here as IS. It is important to state that by intermediate we mean partial crossover at the Fe centre and not an S = 3/2 spin state. The presence of the IS state is also reflected in the octahedral distortion parameters which are again intermediate between pure HS and LS $Fe^{III}$ centres. Increasing the temperature to 295 K results in the Fe2-L bond lengths and octahedral distortion parameters becoming typical of pure HS $Fe^{III}$ (Table 3). Once again the structural data mirrors the magnetic susceptibility studies and confirms that the SCO in **3** involves a spin transition at Fe2 only with Fe1 remaining LS up to 300 K.

Finally, the iodo analogue also contains two crystallographically distinct Fe centres and half a $CH_2Cl_2$ molecule and one disordered MeOH molecule in the asymmetric unit cell and disordered NCS anions. In this instance the Fe-N/O bond lengths for both Fe centres are consistent with a LS state.[16,34] There is a very slight increase in Σ and Θ compared with the low temperature structures of **1**-**3** which most probably stems from the large iodo group on the qsal-I ligand.

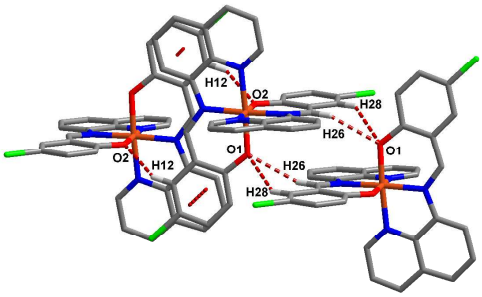


**Figure 4** View of the π-π interactions in [Fe(qsal-Cl)$_2$]NCS·MeOH **2**.

The crystal packing in **1**-**4** is dominated by π-π interactions between the Fe cations which form 1D chains. This is easiest to visualize for **2** as it has the simplest structure. There are two types of π-π interactions supported by one or two C-H···O interactions and denoted Type A and Type B, respectively (Figure 4). The plane to plane distances are 3.287 and 3.349 Å, respectively and indicate that the cationic chains are tightly packed. Type A and Type B π-π interactions are also found in [Fe(qsal)$_2$]NCS but are on average *ca*. 0.25 Å weaker than in **2**. Indeed, it is the presence of these two different π-π interactions that is thought to be responsible for the stepped SCO in [Fe(qsal)$_2$]NCS. Sato *et al*. argue that the π-π interactions form a chain which can be treated as a repeating dimer ··[(B)Fe(A)-(A)Fe(B)]··.[22] Thus, the spin transition can be thought of as proceeding through [LS,LS] ↔ [HS,LS] ↔ [HS,HS] spin isomers. Using a model originally developed by Real and Kahn[35] for $Fe^{II}$ SCO dimers they were able model the asymmetric hysteresis found in [Fe(qsal)$_2$]NCS. As similar π-π interactions occur in **2** it is not unreasonable to suppose that the stepped SCO found in **2** occurs for a similar reason. Moreover, the model also predicts that in situations where the π-π interactions are more similar, the magnetic interactions between the [LS,LS], [HS,LS] and [HS,HS] spin isomers are almost equal resulting in stepped SCO through a 50% HS intermediate with hysteresis in the 1$^{st}$ step only, exactly what is observed in **2**. Although the above is one possible explanation of the stepped SCO in **2**, it is important to state that we cannot rule out symmetry breaking SCO in **2** something that the Mössbauer spectroscopic studies indicate might occur (*vide infra*).

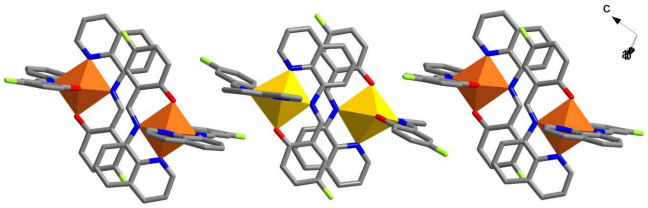


**Figure 5** 1D chain of Fe1-Fe1 (LS-red) and Fe2-Fe2 (HS-yellow) dimers in **1** viewed along the c axis at 200 K.

In the structures of **1** and **3** the presence of two Fe centres complicates matters and although there are two different π-π interactions, these exist only between the Fe1-Fe1 centres or Fe2-Fe2 centres forming closely packed dimers that are connected to one another via C-H···X interactions (X = F, O, Br) with only minimal overlap of the π clouds of neighbouring qsal-X ligands at this part of the chain. In the mixed spin state systems, **1** (200, 270 K) and **3** (295 K), the different spin state dimers form an alternating 1D chain (Figure 5). It is noteworthy that as the temperature increases in **1** there is only a small change in the Fe1-Fe1 π-π interaction from 3.234 to 3.253 Å while the Fe2-Fe2 π-π interaction changes from 3.315 to 3.525 Å due to the complete SCO that occurs at this Fe centre.

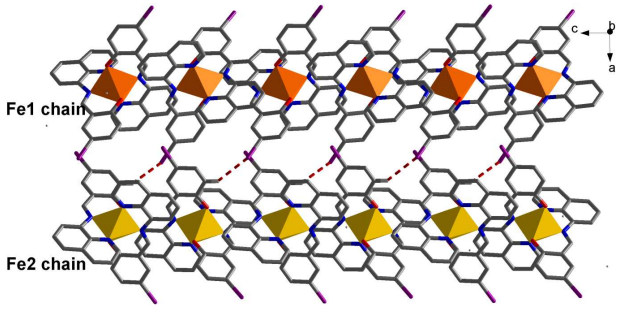


**Figure 6** Fe1 and Fe2 chains in **4** formed from π-π interactions viewed along the *c* axis.

In **3**, at higher temperatures the difference in the Fe2-Fe2 π-π interaction distance is only 0.1 Å, reflecting the smaller change in $\chi_M T$ between the two structures in this instance.

In the case of **4**, although there are again two Fe centres, the packing is different, with individual 1D chains containing only one type of Fe atom (Figure 6). This arrangement of the Fe

atoms may be another contributing factor to the lack of SCO in **4** as all other $[Fe(qsal\text{-}X)_2]NCY$ complexes (Y = S, Se) with two independent Fe centres which exhibit SCO have both Fe1 and Fe2 atoms in the same 1D chain. The π-π distances are 3.305 and 3.399 Å for the Fe1 and Fe2 chains, respectively and are similar to the distances found in $[Fe(qsal\text{-}I)_2]OTf{\cdot}MeOH$.[16] The presence of 1D chains in all of the structures suggests that this is a robust motif which occurs in almost all $[Fe(qsal\text{-}X)_2]^+$ systems and may be used in the design of more complex $[Fe(qsal\text{-}X)_2]^+$ SCO materials.[10,11,16–18,22]

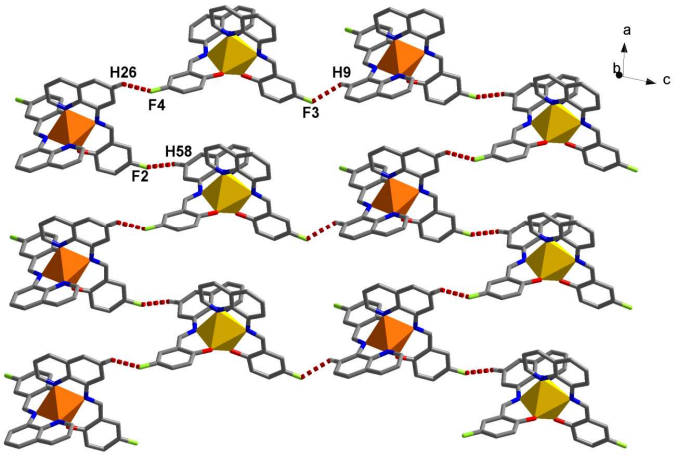


**Figure 7** C-H···F interactions linking neighboring $[Fe(qsal\text{-}F)_2]^+$ cations into 2 dimensions on the *ac* plane at 200 K; Fe1-LS red and Fe2-HS yellow (also observed at 270 K).

Examining the structure beyond the 1D chain motif, we find that these are connected to each other in different ways to create *pseudo* 3D networks. In the case of **1** this is achieved through C-H···F interactions (Figure 7) which form an undulating plane. Interestingly, as the temperature is increased, these C-H···F interactions actually become shorter by on average 0.05 Å as a result of longer π-π interactions in the 1D chains.

In contrast, **2** is composed principally of Cl···π interactions in combination with P4AE interactions.[36] The latter are constructed from two CH···π and one π-π interaction (Figure 8). Despite their very different structures, **3** has many similar features to **2**. In particular, the 1D chains are connected to each other predominantly via Br···π interactions (Figure S6). However, the P4AE interactions are replaced by CH···Br interactions. The Br···π interactions become longer by *ca*. 0.10 Å at room temperature and as there are fewer Br···π interactions than in **2** result in lower cooperativity in **3**.

The iodo complex is again very different, with strong CH···I interactions linking the 1D chains noted above (see Figure 6) to create a 2D plane. The iodo groups are again involved in expanding the structure into the third dimension this time through I···S, C-H···N and C-H···S interactions involving the $NCS^-$ anions.

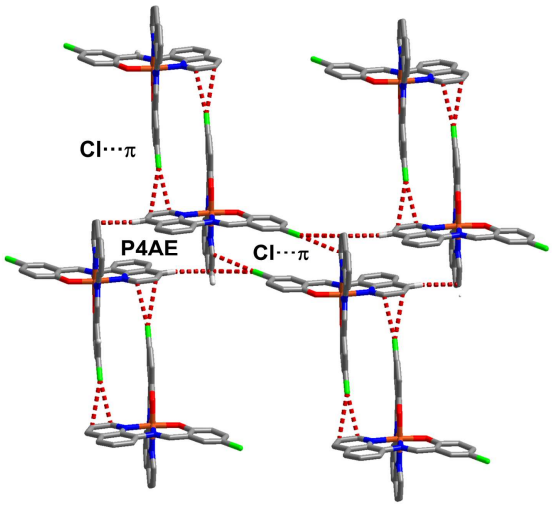


**Figure 8** View of the P4AE and Cl···π interactions that form the 2D plane in **2**.

Comparing the structures of **1**-**4** with that of $[Fe(qsal)_2]NCS$[22] reveals that despite the presence of independent Fe centres in **1**, **3** and **4**, a single Fe centre in the other structures and different solvent molecules the overall packing motif is remarkably constant (Figures 9 and S7). This suggests that the solvent does not radically alter the packing in $[Fe(qsal\text{-}X)_2]^+$ systems, understandable given that the solvents are principally located in between the cationic planes. Viewed down the 1D π-π chains two sets of parallel qsal-X ligands overlap forming a 'central channel' which in the simpler systems is almost square (Figure 9a). In **1** and **3** this channel is rectangular with the Fe1 and Fe2 atoms at alternate corners of the rectangle (Figure 9b).

Examining the packing in more detail it is found that the distance between the $[Fe(qsal\text{-}X)_2]^+$ chains (termed $d_{chain}$ see Figure S8) increases from *ca*. 9.9-10.4 Å for **1** to **4** and correlates with the size of the halogen, unsurprising given the presence of the halogen along this axis.

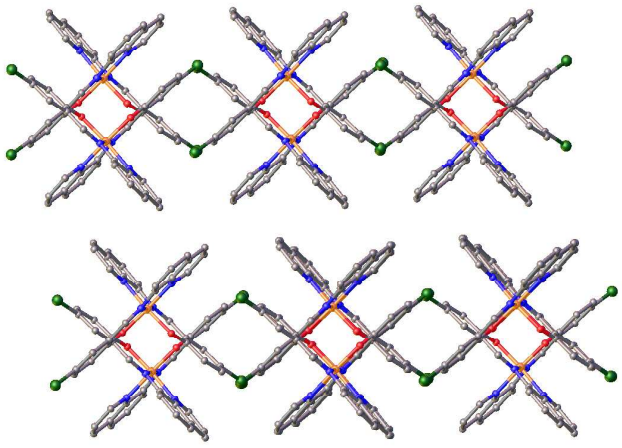

a)

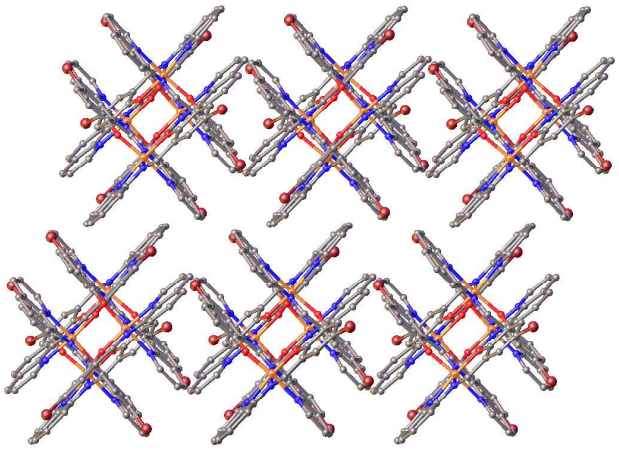

b)

**Figure 9** View of the overall packing in a) **2** and b) **3** (at 123 K) viewed down the 1D π-π chains showing the square and rectangular central channels.

In contrast, the interplanar distance (termed $d_{plane}$, see Figure S7) varies between 12.0-12.8 Å being similar in both **1** and **4** despite the different halogens. In $[Fe(qsal)_2]NCS$, while $d_{plane}$ is *ca*. 12.5 Å, $d_{chain}$ is 9.7 Å and the shortest distance in the $[Fe(qsal\text{-}X)_2]NCS$ series. This may suggest that the tighter packing of the 2D planes in $[Fe(qsal)_2]NCS$ is responsible for the increased cooperativity when compared with **1**-**4**. Overall the structures reveal that the planar qsal-X ligand is essential in the formation of the 1D π-π chains and that the halogen plays an important role in linking the chains to give 3D supramolecular connected networks. However, the number and strength of these interactions is greatest in **1** and **2** and it is this that results in hysteretic spin crossover in these compounds (Tables S4-S6).

### Mössbauer spectroscopic studies of $[Fe(qsal\text{-}X)_2]NCS{\cdot}solvent$

$^{57}$Fe Mössbauer spectra of **1** and **2** were recorded at *ca*. 6 or 7, 100, 200 and 293 K. Spectral parameters are given in Table 5 while the spectra are shown in Figure 10. The room temperature spectrum of **1** reveals a single broad slightly asymmetric doublet at 0.37 mm/s indicative of HS $Fe^{III}$. Interestingly, contrary to expectations based on the magnetic susceptibility data no LS component is visible. Similar inconsistencies between magnetic susceptibility and Mössbauer spectroscopic data have been found in $[Fe(qsal)_2]NCS$ and are thought to be due to the relatively gradual nature of the spin transition.[24] The presence of two crystallographic centres and only one HS doublet has previously been observed for $[Fe(qsal)_2]NCSe$.[10] Cooling the sample to 200 K, results in an increase in intensity and the appearance of a new doublet at δ = 0.17 mm/s with a quadrupole splitting of 2.75 mm/s consistent with LS $Fe^{III}$. The HS:LS ratio is 44:56 and consistent with both the magnetic susceptibility and crystallographic studies which show a 1:1 mixture of HS and LS states. At 100 K the sample is now almost completely LS although a small fraction of HS remains. This also occurs in $[Fe(salpm)_2]ClO_4{\cdot}0.5EtOH$ (salpm = 2-((pyridin-2-ylmethylimino)methyl)phenolate)[37] where, despite 100% LS $Fe^{III}$ from magnetic susceptibility data, a small amount of HS is still present in the Mössbauer spectrum.

**Table 5** $^{57}$Fe Mössbauer spectral parameters of **1** and **2**.

| Compound | T (K) | IS (mm s$^{-1}$)[a] | QS (mm s$^{-1}$)[b] | %HS | %LS |
|---|---|---|---|---|---|
| **1** | 6.9 | 0.21 | 2.79 | - | 87 |
| | | 0.50 | 0.80 | 13 | - |
| | 100 | 0.20 | 2.78 | - | 86 |
| | | 0.48 | 0.73 | 14 | - |
| | 200 | 0.17 | 2.75 | - | 56 |
| | | 0.44 | 0.71 | 44 | - |
| | 293 | 0.37 | 0.55 | 100 | - |
| **2** | 5.9 | 0.20 | 2.65 | - | 90 |
| | | 0.52 | 0.68 | 10 | |
| | 100 | 0.19 | 2.65 | - | 90 |
| | | 0.51 | 0.68 | 10 | - |
| | 200 | 0.17 | 2.57 | - | 67 |
| | | 0.41 | 0.68 | 33 | - |
| | 293[c] | 0.51 | 0.68 | | |

[a]IS = isomer shift relative to α-Fe. [b]QS = quadrupole splitting, estimated errors are ≤ 0.02 mm s$^{-1}$ for IS and QS. [c] Data not fitted due to low signal to noise but isomer shift and quadrupole splitting estimated.

In contrast to **1**, the spectrum at 293 K of **2** is much broader and very similar to that of $[Fe(qsal)_2]NCS$.[24] Although it has been impossible to fit the spectrum due to the high signal to noise ratio it is clear that the sample is mostly HS and the isomer shift and quadrupole splitting can be estimated (see Table 5). At 200 K the LS $Fe^{III}$ doublet is clearly evident at δ = 0.17 mm/s although the HS fraction is lower than would be expected being only 33%. Interestingly, in the symmetry breaking compound $[Fe(nsal_2trien)_2]NCS$ ($nsal_2trien$ = 2,5,8,11-tetraazadodeca-1,11-diene-1,12-diyl-dinaphthalen-2-olate) the amount of HS is also underestimated and has been ascribed to the difference in the recoil-less fractions of the two spin states which are higher for the LS $Fe^{III}$ state due to the shorter and stronger Fe-L bonds of this species.[38] At 100 K, **2** is again mostly LS consistent with the structural and magnetic data. Finally, it is worth noting that following the expected decrease in the isomer shift between 100 and 200 K due to the second-order Doppler effect it is seen to increase again at 293 K and may suggest that a structural change occurs above 200 K.[39]

## Conclusions

In conclusion, we have successfully synthesized a series of $[Fe(qsal\text{-}X)_2]NCS$ complexes which differ in the halogen substituent on the ligand. The fluoro, chloro and bromo derivatives are found to undergo spin crossover with $T_{½}$ increasing as we descend the group, while the iodo analogue is low spin. In the case of the fluoro and chloro derivatives the spin crossover occurs in two steps with hysteresis in the 1$^{st}$ step. Structural studies reveal that for $[Fe(qsal\text{-}F)_2]NCS$ the stepped spin crossover is due to the presence of two crystallographically independent Fe centres meaning that the spin crossover occurs from a [LS-LS] state via a [LS-HS] intermediate to a [HS-HS] state, the first structurally proven stepped spin crossover in $[Fe(qsal\text{-}X)_2]^+$ chemistry. The reason for the stepped SCO in

$[Fe(qsal\text{-}Cl)_2]NCS{\cdot}MeOH$ is less clear and may due to the two types of π-π interactions in the 1D chain or symmetry breaking.

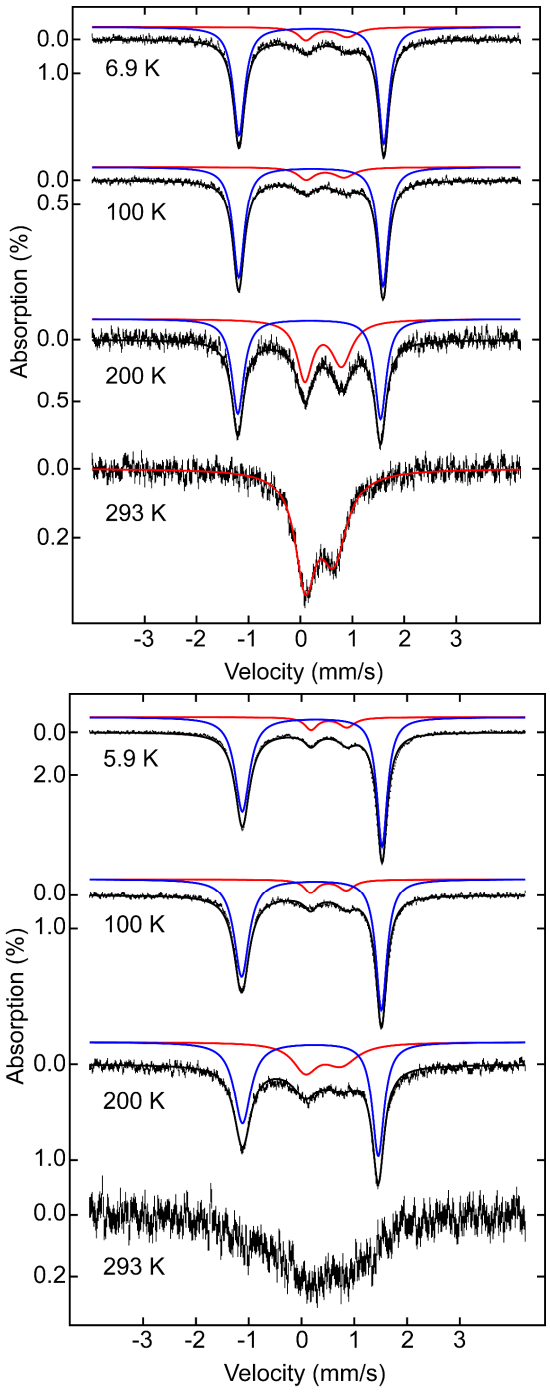


**Figure 10** Mössbauer spectra of **1** (top) and **2** (bottom) between 6 and 293 K.

The lack of SCO in **4** may result from the fact that it crystallizes in monoclinic $P2_1/c$ rather than triclinic $P\bar{1}$, although the arrangement of the independent Fe atoms into separate chains may also influence SCO behaviour. Crystal packing within the structures reveals the presence of extensive π-π interactions in all cases suggesting that for $[Fe(qsal\text{-}X)_2]^+$ compounds this is a robust supramolecular motif. Halogen CH···X and X···π interactions increase the dimensionality of the structures resulting in high cooperativity, particularly in **1** and **2** where the SCO is stepped and abrupt. The overall structural motif is found to be surprisingly constant despite the different halogens and solvent molecules and is most tightly packed in **1**. However, comparison with $[Fe(qsal)_2]NCS$ reveals that introduction of the halogen results in more loosely packed 1D chains within the 2D planes which may be responsible for the less hysteretic SCO in the $[Fe(qsal\text{-}X)_2]NCS{\cdot}sol$ series.

## Experimental

### Materials and Methods

All manipulations were performed in air with reagent grade solvents. All chemicals with the exception of Hqsal-X,[23] were purchased from Aldrich Chemical Company and used as received. Infrared spectra (as KBr discs) were recorded on a Perkin-Elmer Spectrum One infrared spectrophotometer in the range 400-4000 $cm^{-1}$. Electronic spectra were recorded in DMSO at room temperature on a Shimadzu UV-1800 UV-Visible spectrophotometer. Elemental analyses were done using a Eurovector EA3000 analyser by the staff of the School of Chemistry, University of Bristol, UK. ESI-MS were recorded on a Bruker Daltonics 7.0T Apex 4 FTICR Mass Spectrometer by staff at the National University of Singapore.

### Synthesis of $[Fe(qsal\text{-}F)_2]NCS$ 1

$FeCl_3$ (34 mg, 0.2 mmol) was dissolved in MeOH (5 ml) and NaNCS (51 mg, 0.6 mmol) added. The solution was stirred for 5 mins, filtered and then layered on a blank MeOH (3 ml). A solution of Hqsal-F (105 mg, 0.4 mmol) in $CH_2Cl_2$ (2 ml) was in the bottom in which $NEt_3$ (56 µl, 0.4 mmol) had been added as a base. After 3 days black crystals formed which were isolated by filtration, yield 102 mg (79%). $\nu_{max}$(KBr)/$cm^{-1}$ 3056 ($\nu_{CH}$), 2057 ($\nu_{C\equiv N}$), 1600 ($\nu_{C=N}$). $\lambda_{max}$(DMSO)/nm (ε, $dm^3mol^{-1}cm^{-1}$) 421 (11,540), 330 (20,100). m/z (ESI) 586.1 $[Fe(qsal\text{-}F)_2]^+$. Calcd. for (found%) $C_{33}H_{20}N_5F_2FeO_2S$: C, 52.45 (52.49); H, 2.79 (3.13); N, 9.53 % (9.87).

Complexes **2**, **3** and **4** were synthesized in an identical manner to **1**.

### Synthesis of $[Fe(qsal\text{-}Cl)_2]NCS{\cdot}MeOH$ 2

Black crystals, yield 45 mg (33%). $\nu_{max}$(KBr)/$cm^{-1}$ 3056 ($\nu_{CH}$), 2056 ($\nu_{C\equiv N}$), 1601 ($\nu_{C=N}$). $\lambda_{max}$(DMSO)/nm (ε, $dm^3mol^{-1}cm^{-1}$) 421 (12,280), 332 (21,900). m/z (ESI) 618.0 $[Fe(qsal\text{-}Cl)_2]^+$. Calcd. for (found%) $C_{34}H_{24}N_5Cl_2FeO_3S$: C, 52.28 (52.56); H, 3.28 (3.41); N, 8.92 % (8.87).

### Synthesis of $[Fe(qsal\text{-}Br)_2]NCS{\cdot}MeOH$ 3

Black crystals, yield 59 mg (34%). $\nu_{max}$(KBr)/$cm^{-1}$ 3052 ($\nu_{CH}$), 2055 ($\nu_{C\equiv N}$), 1600 ($\nu_{C=N}$). $\lambda_{max}$(DMSO)/nm (ε, $dm^3mol^{-1}cm^{-1}$) 422 (10,660), 330 (19,450). m/z (ESI) 708.0 $[Fe(qsal\text{-}Br)_2]^+$. Calcd. for (found%) $C_{34}H_{24}N_5Br_2FeO_3S$: C, 51.55 (51.15); H, 2.82 (3.03); N, 8.68 % (8.77).

**Synthesis of $[Fe(qsal\text{-}I)_2]NCS{\cdot}0.25CH_2Cl_2{\cdot}0.5MeOH$ 4**

Black crystals, yield 84 mg (49%). $\nu_{max}$(KBr)/cm$^{-1}$ 3054 ($\nu_{CH}$), 2056 ($\nu_{C\equiv N}$), 1599 ($\nu_{C=N}$). $\lambda_{max}$(DMSO)/nm ($\varepsilon$, dm$^3$mol$^{-1}$cm$^{-1}$) 427 (12,590), 332 (24,800). m/z (ESI) 802.0 $[Fe(qsal\text{-}I)_2]^+$. Calcd. for (found%) $C_{33.75}H_{22.5}N_5Cl_{0.5}I_2FeO_{2.5}S$: C, 45.17 (45.30); H, 2.53 (2.34); N, 7.80 % (7.94).

**X-ray crystallography**

Crystal data and data processing parameters for the structures of **1**, **2**, **3** and **4** are given in Table 4. X-ray quality crystals of **1-4** were grown by layering a solution of $Fe(NCS)_3$ in MeOH over a solution of Hqsal-X and $NEt_3$ in $CH_2Cl_2$. Crystals were mounted on a glass fibre using perfluoropolyether oil and cooled rapidly in a stream of cold nitrogen. For **1**, the crystal data was collected at 100, 200 and 270 K at the Australian Synchrotron MX1 beam-line. The data collection and integration were performed within Blu-Ice and XDS software programs. For compounds **2**, **3** and **4**, the diffraction data were collected at 100 K; 123 and 295 K; 123 K, respectively on a Bruker APEXII area detector with graphite monochromated MoK$\alpha$($\lambda$ = 0.71073 Å).[40] After data collection, in each case an empirical absorption correction (SADABS) was applied,[41] and the structures were then solved by direct methods and refined on all $F^2$ data using the SHELX suite of programs.[42] In all cases non-hydrogen atoms were refined with anisotropic thermal parameters; hydrogen atoms were included in calculated positions and refined with isotropic thermal parameters which were *ca*. 1.2 × (aromatic CH) or 1.5 × ($CH_3$, OH) the equivalent isotropic thermal parameters of their parent carbon or oxygen atoms. Pictures were generated using DIAMOND or OLEX-2.[43,44] CCDC 994836 (100 K), 994837 (200 K), 994838 (270 K), 994839, 994840 (123 K), 994841 (295 K) and 994842 contain the supplementary crystallographic data for **1**, **2**, **3** and **4**, respectively. These data can be obtained free of charge from The Cambridge Crystallographic Data Centre via www.ccdc.cam.ac.uk/data_request/cif.

**Magnetic susceptibility and Mössbauer spectroscopic studies**

Samples were stored in the solvent they were crystallized from and filtered just prior to magnetic susceptibility and Mössbauer spectroscopic studies. Data were collected using a Quantum Design MPMS 5 SQUID magnetometer under an applied field of 1 T over the temperature range 340–4 K. The powdered or polycrystalline samples were placed in gel capsules and care was taken to allow long thermal equilibration times at each temperature point. Mössbauer spectra were recorded on a spectrometer from SEE Co. (Science Engineering & Education Co., MN) equipped with a closed cycle refrigerator system from Janis Research Co. and SHI (Sumitomo Heavy Industries Ltd.). Data were collected in constant acceleration mode in transmission geometry. The zero velocity of the Mössbauer spectra refers to the centroid of the room temperature spectrum of a 25 μm metallic iron foil. Analysis of the spectra was conducted using the WMOSS program (SEE Co, formerly WEB Research Co. Edina, MN).

**Solution magnetic susceptibility studies**

$^1$H NMR spectra of **1-4** were recorded at room temperature in d$^6$-DMSO with TMS added as an internal standard against a reference of d$^6$-DMSO with TMS added on a Bruker 300 MHz FT-NMR spectrometer following a modified Evan's method.[28] The reference solvent was placed in a co-axial insert with the solution of the complex in a standard NMR tube. The $\chi_M$T values for **1-4** were then calculated in a standard manner with diamagnetic corrections applied (see ESI).[27,45]

## Acknowledgements

We thank the National Science and Technology Development Agency (grant no.: P-10-11181) and the Thailand Research Fund (RSA5580028) for funding this research. We also thank the Development and Promotion of Science Talents Project for a Ph.D. scholarship to WP. KSM acknowledges support from the Australian Research Council.

## Notes and references

[a] *Molecular Technology Research Unit Cell, School of Science, Walailak University, Thasala, Nakhon Si Thammarat, 80161, Thailand*
[b] *School of Chemistry, Monash University, Clayton, Melbourne, Victoria, 3800, Australia*
[c] *Now at the School of Pharmacy and Biomolecular Sciences, University of Brighton, Brighton, BN2 4GJ, UK*
[d] *School of Physics, Monash University, Clayton, Melbourne, Victoria, 3800, Australia*
[e] *Department of Chemistry & MacDiarmid Institute for Advanced Materials and Nanotechnology, University of Otago, P.O. Box 56, Dunedin 9054, New Zealandf*
[e] *Department of Chemistry, University of Sheffield, Sheffield, S3 7HF, UK*

Electronic Supplementary Information (ESI) available: Supplementary packing diagrams and tables of supramolecular interactions are contained within the ESI. See DOI: 10.1039/b000000x/

1. P. Gütlich and H. A. Goodwin, *Top. Curr. Chem.*, 2004, **233**, 1–47.
2. M. A. Halcrow, Ed., *Spin-Crossover Materials: Properties and Applications*, John Wiley & Sons Ltd., Chichester, 2013.
3. A. Bousseksou, G. Molnár, L. Salmon, and W. Nicolazzi, *Chem. Soc. Rev.*, 2011, **40**, 3313–35.
4. J.-F. Létard, P. Guionneau, and L. Goux-Capes, *Top. Curr. Chem.*, 2004, **235**, 221–249.
5. V. Ksenofontov, A. B. Gaspar, and P. Gütlich, *Top. Curr. Chem.*, 2004, **235**, 23–64.
6. A. Hauser, *Top. Curr. Chem.*, 2004, **234**, 155–198.
7. J.-F. Létard, *J. Mater. Chem.*, 2006, **16**, 2550–59.
8. P. J. van Koningsbruggen, Y. Maeda, and H. Oshio, *Top. Curr. Chem.*, 2004, **233**, 259–324.
9. M. Nihei, T. Shiga, Y. Maeda, and H. Oshio, *Coord. Chem. Rev.*, 2007, **251**, 2606–2621.
10. S. Hayami, Z. Gu, H. Yoshiki, A. Fujishima, and O. Sato, *J. Am. Chem. Soc.*, 2001, **123**, 11644–50.
11. S. Hayami, T. Kawahara, G. Juhasz, K. Kawamura, K. Uehashi, O. Sato, and Y. Maeda, *J. Radioanal. Nucl. Chem.*, 2003, **255**, 443–447.
12. C. Faulmann, S. Dorbes, S. Lampert, K. Jacob, B. Garreau De Bonneval, G. Molnár, A. Bousseksou, J. A. Real, and L. Valade, *Inorg. Chim. Acta*, 2007, **360**, 3870–3878.

13. K. Takahashi, H. Cui, H. Kobayashi, Y. Einaga, and O. Sato, *Chem. Lett.*, 2005, **34**, 1240–1241.
14. K. Takahashi, H.-B. Cui, Y. Okano, H. Kobayashi, Y. Einaga, and O. Sato, *Inorg. Chem.*, 2006, **45**, 5739–5741.
15. K. Takahashi, H. Mori, H. Kobayashi, and O. Sato, *Polyhedron*, 2009, **28**, 1776–1781.
16. D. J. Harding, W. Phonsri, P. Harding, I. A. Gass, K. S. Murray, B. Moubaraki, J. D. Cashion, L. Liu, and S. G. Telfer, *Chem. Commun.*, 2013, **49**, 6340–2.
17. D. J. Harding, D. Sertphon, P. Harding, K. S. Murray, B. Moubaraki, J. D. Cashion, and H. Adams, *Chem. Eur. J.*, 2013, **19**, 1082–90.
18. D. Sertphon, D. J. Harding, P. Harding, K. S. Murray, B. Moubaraki, J. D. Cashion, and H. Adams, *Eur. J. Inorg. Chem.*, 2013, 788–795.
19. S. Floquet, A. J. Simaan, E. Rivière, M. Nierlich, P. Thuéry, J. Ensling, P. Gütlich, J.-J. Girerd, and M.-L. Boillot, *Dalton Trans.*, 2005, 1734–42.
20. M. A. Halcrow, *Chem. Soc. Rev.*, 2011, **40**, 4119–42.
21. N. Nassirinia, S. Amani, S. J. Teat, O. Roubeau, and P. Gamez, *Chem. Commun.*, 2014, **50**, 1003–5.
22. S. Hayami, K. Hiki, T. Kawahara, Y. Maeda, D. Urakami, K. Inoue, M. Ohama, S. Kawata, and O. Sato, *Chem. Eur. J.*, 2009, **15**, 3497–3508.
23. J. Sirirak, W. Phonsri, D. J. Harding, P. Harding, P. Phommon, W. Chaoprasa, R. M. Hendry, T. M. Roseveare, and H. Adams, *J. Mol. Struct.*, 2013, **1036**, 439–446.
24. H. Oshio, K. Kitazaki, J. Mishiro, N. Kato, and Y. Maeda, *J. Chem. Soc., Dalton Trans.*, 1987, 1341–1347.
25. M. P. Shores, C. M. Klug, and S. R. Fiedler, in *Spin Crossover materials: Properties and Applications*, ed. M. A. Halcrow, John Wiley & Sons Ltd., Chichester, 2013, pp. 281–301.
26. D. F. Evans, *J. Chem. Soc.*, 1959, 2003.
27. E. M. Schubert, *J. Chem. Educ.*, 1992, **69**, 62.
28. T. H. Crawford and J. Swanson, *J. Chem. Educ.*, 1971, **48**, 382–386.
29. B. Djukic, P. A. Dube, F. Razavi, T. Seda, H. A. Jenkins, J. F. Britten, and M. T. Lemaire, *Inorg. Chem.*, 2009, **48**, 699–707.
30. J. C. Dias, B. Vieira, I. C. Santos, L. C. J. Pereira, and V. Da Gama, *Inorg. Chim. Acta*, 2009, **362**, 2076–2079.
31. J. K. McCusker, A. L. Rheingold, and D. N. Hendrickson, *Inorg. Chem.*, 1996, **35**, 2100–2112.
32. M. Marchivie, P. Guionneau, J. F. Létard, and D. Chasseau, *Acta Crystallogr. Sect. B Struct. Sci.*, 2005, **61**, 25–8.
33. A. I. S. Neves, J. C. Dias, B. J. C. Vieira, I. S. Santos, M. B. Castelo Branco, L. C. J. Pereira, J. C. Waerenborgh, M. Almeida, D. Belo, and V. Da Gama, *CrystEngComm*, 2009, **11**, 2160–68.
34. K. Fukuroi, K. Takahashi, T. Mochida, T. Sakurai, H. Ohta, T. Yamamoto, Y. Einaga, and H. Mori, *Angew. Chem. Int. Ed.*, 2014, **53**, 1983–6.
35. J. A. Real, H. Bolvin, A. Bousseksou, A. Dworkin, O. Kahn, F. Varret, and J. Zarembowitch, *J. Am. Chem. Soc.*, 1992, **114**, 4650–4658.
36. V. Russell, M. Scudder, and I. Dance, *J. Chem. Soc., Dalton Trans.*, 2001, 789–799.
37. K. D. Murnaghan, C. Carbonera, L. Toupet, M. Griffin, M. M. Dîrtu, C. Desplanches, Y. Garcia, E. Collet, J.-F. Létard, and G. G. Morgan, *Chem. Eur. J.*, 2014, **20**, 5613–18.
38. B. J. C. Vieira, J. T. Coutinho, I. C. Santos, L. C. J. Pereira, J. C. Waerenborgh, and V. da Gama, *Inorg. Chem.*, 2013, **52**, 3845–50.
39. P. Gütlich, E. Bill, and A. X. Trautwein, *Mošsbauer Spectroscopy and Transition Metal Chemistry*, Springer-Verlag, Berlin/Heidelberg, 2011.
40. Bruker, APEXII, *Bruker AXS Inc*., Madison, WI, USA, 2005.
41. SADABS and SAINT, *Bruker AXS Inc*., Madison, WI, USA, 2003.
42. G. M. Sheldrick, *Acta Cryst.*, 2008, **A64**, 112–22.
43. K. Brandenberg and H. Putz, DIAMOND, *Crystal Impact*, Bonn, Germany, 2006.
44. O. V. Dolomanov, L. J. Bourhis, R. J. Gildea, J. A. K. Howard, and H. Puschmann, *J. Appl. Cryst.*, 2009, **42**, 339–42.
45. G. A. Bain and J. F. Berry, *J. Chem. Educ.*, 2008, **85**, 532.



 